

Distributed Image Compression with Multimodal Side Information at Extremely Low Bitrates

Guojun Xu, Mingyang Zhang, Jianwen Xiang, Cheng Tan, Yanchao Yang, Junwei Zhou*
 School of Computer Science and Artificial Intelligence, Wuhan University of Technology
 guojunxu@whut.edu.cn, junweizhou@msn.com

Abstract

Distributed Image Compression (DIC) is crucial for multi-view transmission, especially when operating at extremely low bitrates (< 0.1 bpp). Its core challenge is effectively utilizing side information to achieve high-quality reconstruction under strict bitrate budgets. However, existing DIC approaches struggle to exploit global context and object-level details from side information, leading to local blurring and the loss of fine details in the reconstruction. To address these limitations, we propose a Multimodal DIC framework (MDIC), which, for the first time, leverages side information in a multimodal manner into the DIC paradigm, effectively preserving fine-grained local details and enhancing global perceptual quality in reconstructed images. Specifically, we introduce a text-to-image diffusion-based decoder conditioned on textual side information extracted from correlated images to capture shared global semantics. Moreover, we design a feature-mask generator, supervised by a multimodal fine-grained alignment task, to strengthen the exploitation of visual side information. The generated mask serves two purposes: first, it guides the extraction of fine-grained details from losslessly transmitted side information to preserve the semantic consistency of reconstructed details; second, it regulates the extraction of clustered feature representations from the quantized VQ-VAE embeddings, compensating for category information lost under the extreme compression of the primary image. Extensive experiments on the widely used KITTI Stereo and Cityscapes datasets demonstrate that MDIC achieves state-of-the-art perceptual quality at extremely low bitrates.

1. Introduction

Distributed Image Compression (DIC) transmits one view losslessly and leverages it as side information to assist in the reconstruction of other compressed views at the decoder [20, 21, 32]. In multi-view distributed scenarios such

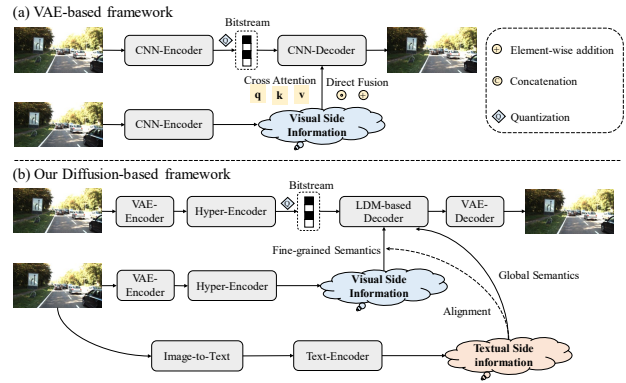


Figure 1. (a) The existing VAE-based distributed coding framework only with visual side information [20, 21, 32, 40]. (b) Our diffusion-based pipeline with multimodal side information.

as multi-camera surveillance and 3D scene reconstruction, DIC is particularly important without requiring interaction among encoder devices, theoretically can achieve compression efficiency comparable to joint coding [29, 35]. Given their bandwidth-constrained application scenarios and reliance on side information, the DIC algorithms are primarily suited to extremely low bitrates (< 0.1 bits per pixel (bpp)).

The main challenge in DIC lies in effectively utilizing the side information at the decoder, which is highly correlated with the compressed image features [20, 21, 37, 40]. It is crucial to fully exploit informative correlated features while suppressing irrelevant or redundant ones that may interfere with reconstruction. Nevertheless, separating these two types of information is non-trivial due to the complexity and diversity of multi-view object-level details. Moreover, the varying importance of fine-grained information across different regions and objects makes it difficult to balance the model’s attention effectively.

As illustrated in Fig. 1 (a), most existing DIC methods are built upon a VAE framework, where side information is fused through global cross-attention modules [21, 32, 38, 40], enabling interaction between compressed features

* Junwei Zhou is the corresponding author.



Figure 2. Comparison of reconstruction performance by joint coding method BiSIC [17] and CAMSIC [41], the DIC method LDMIC [40], the LIC method Perco [3], DiffEIC [14] and RDEIC [15], and the proposed MDIC. bpp_k and bpp_c are the compressed bits per pixel (bpp) of these methods in two images.

and the auxiliary view. However, under extremely low bitrates, the transmitted features are highly degraded and contain far less information than the side input. As a result, the attention mechanism can focus only on signals correlated with the limited transmitted content, making it difficult to recover lost object-level details during compression. Moreover, these methods prioritize pixel-wise fidelity between reconstructed and original images [1, 20, 21, 38, 40], while neglecting the perceptual quality of the reconstruction. When detailed information is missing, they tend to compensate by averaging correlated cues rather than efficiently utilizing side information aligned with the compressed content’s detailed semantics. At extremely low bitrates, this results in excessively smooth reconstructions, exhibiting local blurring, as shown in Fig. 2. Representative multi-view coding frameworks such as LDMIC [40] and BiSIC [17] rely heavily on attention mechanisms but insufficiently exploit fine-grained side information, resulting in blurred textures and degraded perceptual quality.

Recently, perception-oriented compression frameworks [3, 10, 11, 14, 19, 25, 36] have achieved remarkable progress in Learned Image Compression (LIC), generating high-quality reconstructions from limited information under semantic guidance. Leveraging large-scale pre-training, these models deliver strong perceptual fidelity on benchmark datasets [16, 23, 42]. However, these methods fail to achieve satisfactory performance when applied to distributed scenarios due to the limited scale of trainable multi-view datasets and the absence of dedicated side-information modeling. As illustrated in Fig. 2, Perco [3], DiffEIC [14], and RDEIC [15] are diffusion-based LIC framework. Although it yields visually appealing reconstructions, it often produces details inconsistent with the original image and suffers from local distortions.

To address these challenges, we propose a Multimodal

Distributed Image Compression (MDIC) framework built upon a pre-trained Latent Diffusion Model (LDM), as illustrated in Fig. 1 (b), where side information is leveraged in a multimodal form. During training, a feature-mask generator, supervised by a multimodal alignment task, is introduced to produce a region-aware mask that adaptively regulates the use of side information. The multimodal alignment provides object-level semantic supervision, guiding the visual mask to capture fine-grained cues with varying semantic importance.

We further incorporate VQ-VAE quantization [30] to cluster the core category representations. The generated visual mask is applied to the quantized side information to recover category information that is lost during extreme compression. On the other hand, it is applied to the unquantized side information to preserve fine-grained details around key object regions while constraining the reconstructed image to remain semantically consistent with the original content. As illustrated in Fig. 2, the proposed MDIC achieves superior perceptual quality while maintaining comparable pixel-wise fidelity.

The contributions of our work are as follows:

- We propose a novel Multimodal DIC (MDIC) framework that, for the first time, leverages multimodal side information to guide distributed image reconstruction, enabling richer semantic priors and fine-grained detail preservation at extremely low bitrates.
- We introduce an object-level text prediction task to supervise the proposed feature-mask generator. By enforcing semantic consistency at the object level, the task guides the mask to function as an information gate, selectively retaining category cues and fine-grained structural details.
- The proposed MDIC achieves impressive perceptual quality at extremely low bitrates, outperforming both existing DIC methods and perception-oriented LIC ap-

proaches across multiple perceptual evaluation metrics.

2. Related Work

2.1. Distributed Image Compression

Distributed Image Compression (DIC) is grounded in the Slepian-Wolf theory [29], which shows that distributed coding can match the efficiency of joint coding, and is later extended to lossy compression by Wyner and Ziv [35].

As illustrated in Fig. 3 (a), learned DIC frameworks predominantly operate under an asymmetric paradigm, where one view is transmitted losslessly to the destination (e.g., central storage or processing unit) and serves as side information for reconstructing other lossy compressed views. The side information incurs no additional bitrate and requires no interaction among encoder-side devices [20, 32]. Representative methods include NDIC [20], which extracts shared information from primary and correlated views for decoder-side fusion, and ATN [21], which leverages a cross-attention module to integrate side information during decoding. LDMIC [40] further extends this idea with a joint context module to better exploit multi-view correlations.

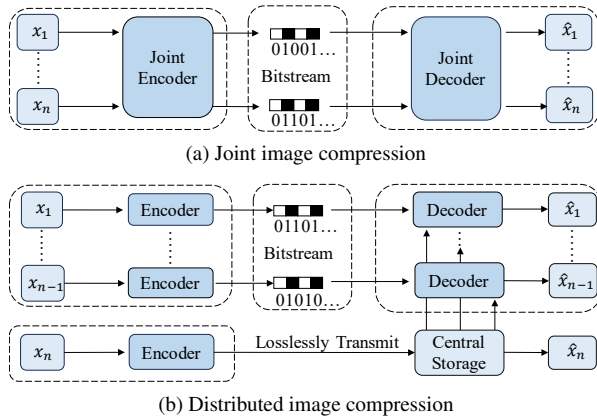


Figure 3. Different compressors for multi-view images.

Fig. 3 (b) illustrates a joint coding paradigm, a symmetrical framework in which multi-view images are encoded and decoded jointly, commonly applied to Stereo Image Compression (SIC) [24, 41]. SASIC [33] uses a stereo attention module to connect left and right views during decoding. ECSIC [34] explicitly models the mutual information shared across stereo images to improve coding efficiency. BiSIC [17] employs 3D convolutions and bidirectional attention to extract both local and global contextual features.

Despite significant progress in improving distortion metrics such as PSNR [12] and MS-SSIM [31], these methods suffer from regional and even global blurring at extremely low bitrates. This is because they focus on pixel-wise reconstruction fidelity while neglecting alignment between the distributions of the reconstructed and original images,

thereby underutilizing distribution-consistent cues in the side information. In contrast, our approach leverages multimodal side information, in which textual representations capture global distributional information between multi-view images. Benefiting from the multimodal integration and detail-rich generation capability of the pre-trained LDM, our method avoids local pixel averaging and yields sharper reconstructions from highly compressed data.

2.2. Diffusion-based Compressors

Diffusion-based image compression methods are mainly designed for extremely low bitrates, aiming to maintain distributional consistency between the original and reconstructed images to achieve high perceptual quality [3, 14, 15]. Perco [3] first introduces a pre-trained text-to-image diffusion model to the decoder of the LIC task. DiffEIC [14] further proposes a two-stage framework that leverages the strong generative capacity of diffusion models for realistic reconstruction at ultra-low bitrates. RDEIC [15] employs compressed feature initialization and residual diffusion, using noisy latent features to accelerate denoising and improve reconstruction efficiency.

Diffusion-based compressors recover rich global semantics even at extremely low bitrates, naturally benefiting DIC by enabling the separation of global and fine-grained cues within side information. Motivated by this, we propose a DIC framework built upon a pre-trained text-to-image diffusion model, which introduces an object-level multimodal alignment task to generate semantic masks and a masked mechanism to efficiently exploit side information.

3. Method

3.1. Overview of the Proposed Framework

The overall architecture of the proposed MDIC is illustrated in Fig. 4. At the encoder side, a frozen pre-trained VAE encodes the images into a latent space. The encoded features are then refined and compressed using a convolutional and linear-attention hybrid module, producing deep semantic representations for subsequent VQ-VAE quantization and transmission. The overall process is:

$$\begin{cases} z_{Lx} = E_{vae}(I_x), \\ \hat{z}_x = VQ(H_{ax}(z_{Lx})), \end{cases} \quad (1)$$

$$\begin{cases} z_y = H_{ay}(E_{vae}(I_y)), \\ \hat{z}_y = VQ(z_y), \end{cases} \quad (2)$$

$$z_{text} = E_{clip}(B_2(I_y)), \quad (3)$$

where E_{vae} denotes the pre-trained VAE encoder, VQ represents the VQ-VAE quantization module [30], H_{ax} and H_{ay} are the HyperAlign module that is similar to Perco [3], B_2 refers to the BLIP-2 captioning model [13], and E_{clip}

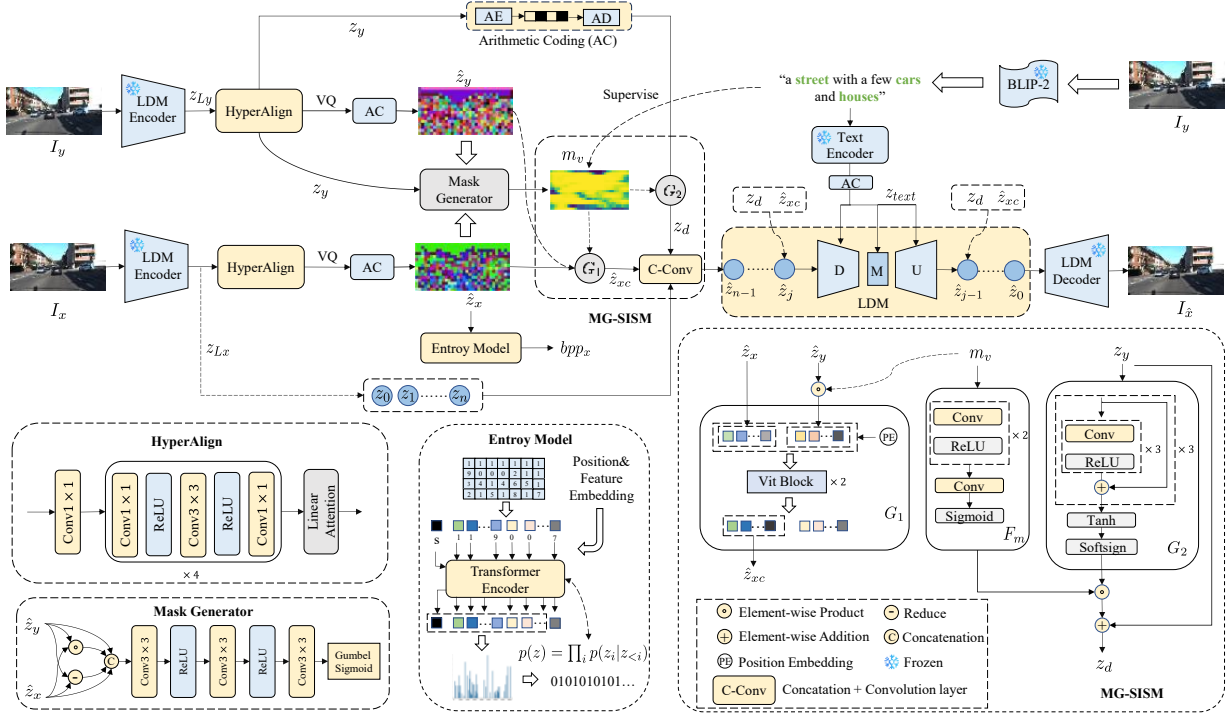


Figure 4. Overview of the proposed MDIC framework. The input view I_x is lossy-compressed, while the correlated view I_y is transmitted losslessly as side information available only at the decoder. Both I_x and I_y are encoded into latent spaces by the LDM encoder [27], producing z_{Lx} and z_{Ly} , which are further refined by the HyperAlign module into z_x and z_y . VQ-VAE quantization [30] is applied for compression and feature clustering, yielding \hat{z}_x and \hat{z}_y . A Transformer-based autoregressive entropy model [32] estimates the bitrate bpp_x . The BLIP-2 captioning model [13] generates textual descriptions from I_y , which are then encoded into z_{text} to provide global semantic guidance. The Arithmetic Encoding (AE) further converts the \hat{z}_x , \hat{z}_y , z_y , and z_{text} into a binary bitstream, with the Arithmetic Decoding (AD) performing the inverse operation. Under the supervision of z_{text} , a visual mask m_v is generated and integrated into the Mask-Gated Side Information Supplementary Module (MG-SISM): gate G_1 fuses \hat{z}_y to restore categorical information lost in \hat{z}_x , while gate G_2 extracts fine-grained object details from z_y . After a denoising process guided by multimodal side information (z_d , \hat{z}_{xc} , and z_{text}), the final reconstruction $I_{\hat{x}}$ is obtained by decoding the denoised latent variable \hat{z}_0 with the LDM decoder.

denotes the CLIP text encoder [26]. To estimate the coding cost, a Transformer-based autoregressive entropy model [32] is employed to model the probability distribution of \hat{z}_x , from which the average bitrate bpp_x is derived.

On the decoder side, the Visual Mask Generation Module in Text Supervision (VMGM-TS) generates a visual feature mask to effectively modulate the available visual side information by the Mask-Gated Side Information Supplementary Module (MG-SISM). Then the textual side information z_{text} provides global semantic guidance for the denoising process, while the visual side information focuses on reconstructing fine-grained local details. The combined guidance enables semantically consistent reconstruction, and the final image is obtained through a VAE decoder.

3.2. Visual Mask Generation Module in Text Supervision (VMGM-TS)

To preserve fine-grained details while suppressing redundant multi-view discrepancies, we introduce a Visual Mask

Generation Module in Text Supervision (VMGM-TS), as illustrated in Fig. 5. The module aligns the generated visual mask with object-level textual semantics, enabling end-to-end learning with visual side information. It identifies spatial regions of target objects and captures their semantic representations, facilitating faithful reconstruction of text-referred content.

To capture fine-grained object semantics, we construct a vocabulary of the N most frequent object nouns in the dataset. During training, object-related words in the image captions are replaced with special mask tokens to form object-masked text. The contextual representations of these masked words are jointly modeled with their corresponding visual masks via an autoregressive-based fusion architecture, enabling alignment between textual context and the visual regions of the same object and facilitating deeper object-level semantic learning beyond explicit word-object correspondences. During the inference phase, the mask can be directly obtained from the trained mask generator.

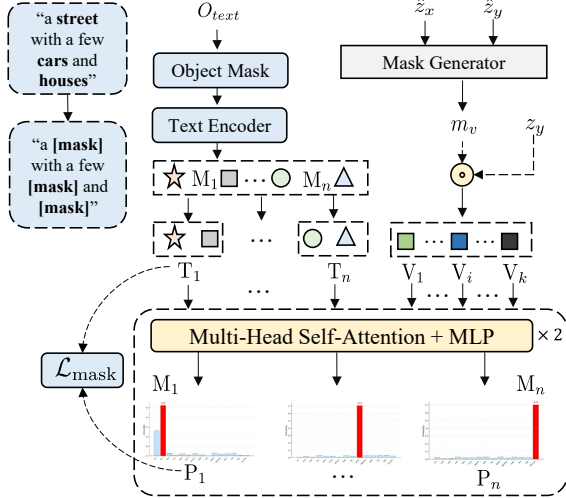


Figure 5. Visual Mask Generation Module in Text Supervision (VMGM-TS). This module is regarded as an auxiliary task that supervises the Mask Generator, enabling alignment between the object-level visual features and the masked text vocabulary.

The overall mask-generating process is as follows:

$$F_{diff} = |\hat{z}_x - \hat{z}_y|, \quad F_{prod} = \hat{z}_x \odot \hat{z}_y, \quad (4)$$

$$logits = \text{Conv}(\text{concat}(\hat{z}_x, \hat{z}_y, F_{diff}, F_{prod})), \quad (5)$$

$$g = -\log(-\log(U + \epsilon) + \epsilon), \quad U \sim \mathcal{U}(0, 1), \quad (6)$$

$$m = \sigma\left(\frac{logits + g}{\tau}\right), \quad (7)$$

$$m_v = \mathbb{I}(m > \theta) + sg(m - \mathbb{I}(m > \theta)), \quad (8)$$

where F_{diff} and F_{prod} represent the element-wise difference and product capturing disparity and similarity cues. The $\text{Conv}(\cdot)$ denotes a three-layer convolutional module with ReLU activation that outputs the values of the mask, as shown in Fig. 4. The g is the Gumbel noise sampled [9] from a uniform distribution $\mathcal{U}(0, 1)$, and τ is the temperature controlling the smoothness of the Gumbel-Sigmoid function. The θ is the hard sampling threshold, and $\mathbb{I}(\cdot)$ is the indicator function for binary masking, $sg(\cdot)$ represents the stop-gradient operation.

The auxiliary supervision process for the mask generator is as follows:

$$M_{text} = M(O_{text}), \quad (9)$$

$$\{T_1, \dots, T_n\} = T_{encoder}(M_{text}), \quad (10)$$

$$\{V_1, \dots, V_k\} = P_{token}(m_v \odot z_y), \quad (11)$$

$$\{P_1, \dots, P_n\} = P_{MSA}(T_1, \dots, T_n, V_1, \dots, V_k), \quad (12)$$

where M represents the Object Mask. O_{text} is the orange text and M_{text} is the masked text. P_{token} tokenizes the visual features. $T_{encoder}$ encodes the context of masked vocabulary to $\{T_1, \dots, T_n\}$, $n \in 1, 2, \dots, N$. $\{V_1, \dots, V_k\}$ are

the tokenized visual features obtained by fusing the visual mask m_v with side information z_y . P_{MSA} is a mask predictor based on the multi-head self-attention. $\{P_1, \dots, P_n\}$ is the prediction of the masked text.

3.3. Mask-Gated Side Information Supplementary Module (MG-SISM)

To further compensate for the loss of categorical information and rich object-level details caused by quantization during compression, we introduce a Mask-Gated Side Information Supplementary Module (MG-SISM). The brief mathematical formulation for MG-SISM can be given as follows:

$$\hat{z}_{xc} = G_1(\hat{z}_x, \hat{z}_y \odot m_v), \quad (13)$$

$$z_d = z_y + G_2(z_y) \odot F_m(m_v). \quad (14)$$

As illustrated in Fig. 4, VQ-VAE quantization compresses the information while simultaneously clustering image features into a structured latent space, thereby facilitating global reconstruction during denoising. The visual mask m_v is first applied to the quantized side information \hat{z}_y to focus on category-related regions. These masked features interact with the quantized latent representation of the main image through visual Transformer blocks [6], producing semantically enriched category features \hat{z}_{xc} .

A gating mechanism further regulates the losslessly transmitted visual side information z_y , ensuring that fine-grained object-level details receive maximal attention while suppressing redundant or variant information. This gated output z_d enhances both semantic consistency and perceptual fidelity in the reconstructed images.

3.4. Decoder with Latent Diffusion Model

We employ a multimodal-conditioned denoising diffusion model to learn the underlying data distribution, where visual side information provides fine-grained details and overall categorical features, while textual side information guides the denoising toward semantically consistent reconstruction (Fig. 4). The diffusion and denoising process is as follows:

$$z_t = \sqrt{\hat{\alpha}_t} z_{Lx} + \sqrt{1 - \hat{\alpha}_t} \varepsilon, \quad (15)$$

$$q(z_t | z_{t-1}) = \mathcal{N}(z_t; \sqrt{1 - \beta_t} z_{t-1}, \beta_t I), \quad (16)$$

$$p_\theta(z_{t-1} | z_t) = \mathcal{N}(z_{t-1}; \mu_\theta(z_t, Z_{cond}, t), \beta_t I). \quad (17)$$

Here, (15) and (16) represent the process of forward noise addition. $\varepsilon \sim \mathcal{N}(0, 1)$ is standard Gaussian noise, $t \in \{1, \dots, T\}$ denotes the diffusion timestep, $\beta_t \in (0, 1)$ represents the variance schedule, and $\hat{\alpha}_t = \prod_{i=1}^t (1 - \beta_i)$. The conditional multimodal side information is defined as $Z_{cond} = \{z_d, \hat{z}_{xc}, z_{text}\}$, where z_d , \hat{z}_{xc} , and z_{text} correspond to fine-grained detail semantics, clustered category features, and global textual information, respectively. During the denoising process, a neural network $\mu_\theta(\cdot)$ predicts

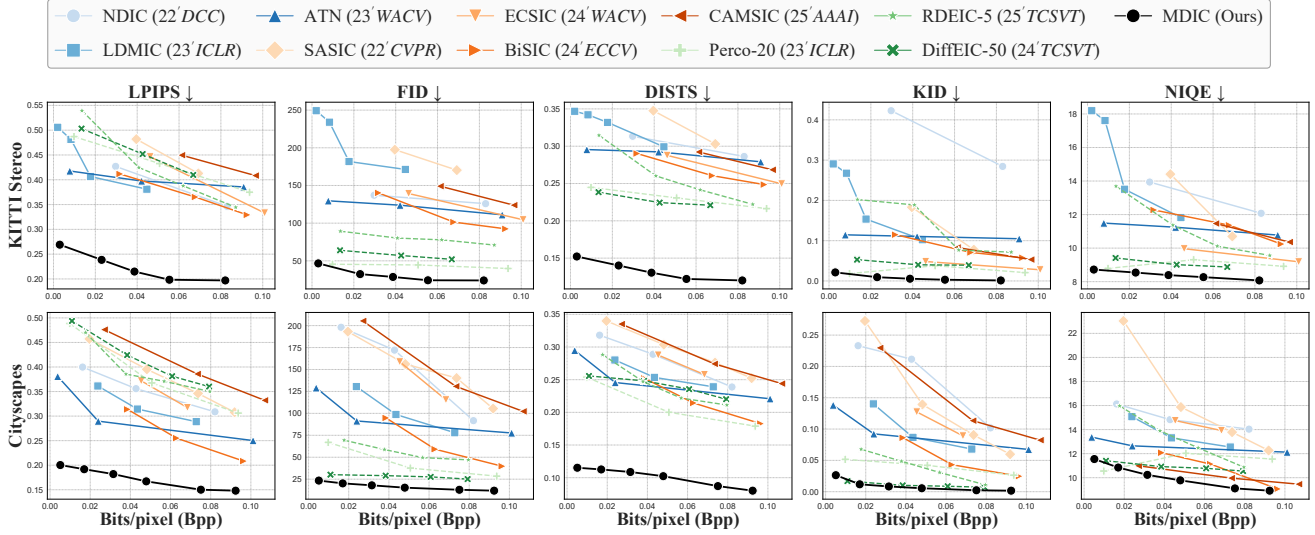


Figure 6. Perception evaluation of MDIC and other DIC, SIC, and LIC methods on KITTI Stereo and Cityscapes datasets.

the posterior mean based on the noisy input z_t , the conditioning information Z_{cond} , and the diffusion timestep t .

After the iterative denoising process, the latent representation \hat{z}_0 is obtained. We then employ a pre-trained VAE decoder D_{vae} to reconstruct the image from the latent space:

$$I_{\hat{x}} = D_{vae}(\hat{z}_0), \quad (18)$$

where $I_{\hat{x}}$ denotes the reconstructed image.

3.5. Loss Function

We adopt the noise prediction objective as distortion loss:

$$\mathcal{L}_{diff} = \mathbb{E}_{z_0, \epsilon, t} [\|\epsilon - \epsilon_\theta(z_t, t, Z_{cond})\|_2^2], \quad (19)$$

where z_0 denotes the latent representation initialized from z_{Lx} , $\epsilon \sim \mathcal{N}(0, I)$ denotes the Gaussian noise, and z_t is obtained via the forward diffusion process in (15). The function $\epsilon_\theta(\cdot)$ is implemented using a U-Net [28] architecture (Fig. 4), which consists of a downsampling encoder (D), a middle block (M), and an upsampling decoder (U).

Our main function \mathcal{L} consists of mask auxiliary loss \mathcal{L}_{mask} , vector quantization loss \mathcal{L}_{VQ} , and rate-distortion tradeoff loss \mathcal{L}_{RD} . They are defined as follows:

$$\mathcal{L}_{mask} = \frac{1}{n} \sum_{i=1}^n CE(P_i, T_i), \quad (20)$$

$$\mathcal{L}_{VQ} = \mathbb{E}_{z_x} [\|sg(z_x) - \hat{z}_x\|_2^2 + \|sg(\hat{z}_x) - z_x\|_2^2], \quad (21)$$

$$\mathcal{L}_{RD} = E_{I_x} [\lambda \cdot E_{\hat{z}_x \sim p(\hat{z}_x | I_x)} [-\log_2(p(\hat{z}_x))] + \mathcal{L}_{diff}], \quad (22)$$

$$\mathcal{L} = \mathcal{L}_{VQ} + \lambda_{mask} \cdot \mathcal{L}_{mask} + \mathcal{L}_{RD}, \quad (23)$$

where \mathcal{L}_{mask} supervises the mask generator by measuring the cross-entropy loss between the predicted mask P_i and

the ground-truth mask T_i over all n samples. \mathcal{L}_{VQ} follows the standard VQ-VAE formulation, which consists of a codebook commitment term and a codebook embedding term. The Rate-Distortion loss \mathcal{L}_{RD} is the core loss of image compression, balancing the trade-off between bitrate and reconstruction quality by hyperparameter λ . $p(\hat{z}_x)$ is the probability distribution of \hat{z}_x , and λ_{mask} is set to 0.1.

4. Experiments

4.1. Experimental Settings

Training Setup and Datasets. We train and evaluate our model on the KITTI Stereo [7] and Cityscapes [4] datasets. Following NDIC [20], 1576 image pairs from KITTI are used for training, and 790 pairs are used for validation and testing. For Cityscapes, we use 2975 image pairs for training, 500 for validation, and 1525 for testing. All KITTI images are center-cropped to 370×740 and then downsampled to 128×256 , while the Cityscapes images are directly resized to the same resolution.

Our model is trained on four NVIDIA L40 GPUs with a batch size of 8 using the AdamW optimizer. The learning rate follows a constant with a warmup schedule, where it linearly increases to 8×10^{-5} during the first 10000 iterations and remains constant thereafter. Training is conducted for an average of 200 epochs per data point. During inference, the number of diffusion steps is set to 10, and the hard sampling threshold θ is 0.2. We construct the vocabulary consisting of the 14 most frequent object nouns in both datasets. Based on the Rate-Distortion tradeoff setting of Perco [3], we further set the hyperparameter λ to $\{0.1, 10\}$.

Evaluation Metrics. We evaluate performance using LPIPS [39], FID [8], DISTS [5], KID [2], NIQE [22],

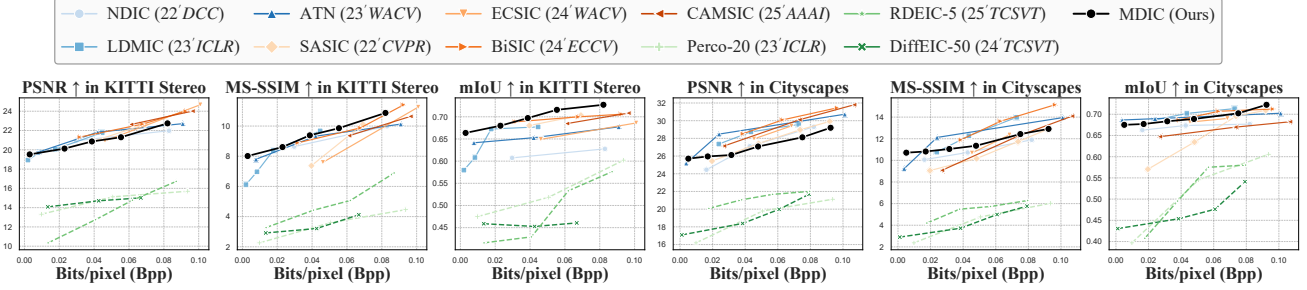


Figure 7. Distortion evaluation of MDIC and other DIC, SIC, and LIC methods on KITTI Stereo and Cityscapes datasets.



Figure 8. Visualization results on KITTI Stereo and Cityscapes datasets. Each row compares two methods (three images per method). Numbers below the images indicate (Bpp, PSNR, LPIPS). Ground Truth includes symbol conventions: \uparrow =higher better, \downarrow =lower better.

as well as PSNR [12] and MS-SSIM [31]. To assess the object-level semantic consistency, we further employ the mean Intersection over Union (mIoU) metric [18]. PSNR and MS-SSIM serve as the primary distortion metrics in DIC, whereas LPIPS, FID, KID, NIQE, and DISTs are commonly used to assess the perceptual realism. Since low-level distortion metrics become less meaningful at extremely low bitrates [3], and our DIC framework is primarily designed for such low-rate scenarios, perceptual quality metrics are adopted as the main evaluation criteria.

Baselines. We reimplement NDIC [20], LDMIC [40], and ATN [21], where LDMIC [40] is commonly used as a representative DIC baseline. For comparison with joint coding approaches, we include SASIC [33], ECSIC [34], CAMSIC [41], and BiSIC [17]. To further compare with diffusion-based image compression frameworks, we evaluate Perco [3], DiffEIC [14], and RDEIC [15], among which Perco serves as a baseline in LIC methods based on pre-trained latent diffusion models.

4.2. Main Results

Comparisons With State-of-the-art (SOTA) Methods. We compare the proposed MDIC with SOTA DIC and SIC

methods, all of which take multi-view images as input for compression and reconstruction. Since our work is the first to introduce a perceptually optimized diffusion-based architecture into DIC, we further include benchmark perception-oriented LIC methods for comparison.

As shown in Fig. 6, MDIC achieves the best performance across all perceptual quality metrics in the KITTI Stereo and Cityscapes datasets, significantly surpassing previous DIC approaches. Even when compared with joint coding schemes in SIC, MDIC demonstrates notable improvements in perceptual quality. Moreover, perception-oriented LIC methods, despite the absence of side information, still perform competitively on most perceptual metrics. This is because perceptual optimization aims to align the distribution of the reconstructed image with that of the original one, rather than ensuring pixel-wise fidelity. To comprehensively assess the effectiveness of our method, we further compare it with existing approaches using distortion metrics. As illustrated in Fig. 7, our method achieves the highest MS-SSIM and mIoU on the KITTI Stereo dataset. Although MDIC achieves a lower PSNR than distortion-oriented methods, it attains a comparable mIoU to the best of them, demonstrating its effectiveness in preserving

object-level details. Our distortion metrics significantly outperform other diffusion-based LIC methods, demonstrating its superior ability to maintain semantic consistency. Moreover, at extremely low bitrates, conventional distortion metrics become less meaningful [3].

Visualize comparisons. As illustrated in Fig. 8, we provide qualitative visual comparisons among various methods. At extremely low bitrates, existing DIC methods, such as ATN, tend to suffer from severe local or even global blurring, which significantly degrades perceptual quality. Although joint coding approaches like BiSIC can partially alleviate this issue, they often introduce noticeable local distortions and artifact patterns. Diffusion-based LIC methods, such as Perco and RDEIC, on the other hand, effectively reduce blurring but frequently produce locally inconsistent semantics due to the lack of fine-grained alignment. In contrast, the proposed MDIC effectively avoids these problems. Benefiting from fine-grained perception and multimodal alignment strategies, our method achieves superior perceptual quality with consistent semantics across both global and local regions.

4.3. Ablation Studies

Side information \hat{z}_{xc} and z_d . As shown in Table 1, we conduct ablation experiments on two types of image side information. When the fine-grained semantic information z_d is removed, the diffusion model tends to generate object details (e.g., color or contour) that are inconsistent with the original image. This leads to a noticeable drop in pixel-level fidelity, while having relatively little effect on perceptual consistency. When the category feature information \hat{z}_{xc} is missing, the diffusion model can only generate content from a limited set of categories. Under extremely low bitrates, the absence of sufficient categories severely affects both global and local reconstruction quality of the generated images.

Table 1. Ablation study of \hat{z}_{xc} and z_d . BD-Quality denotes the average changes of various quality metrics compared with the MDIC baseline at identical bitrates. Higher is better (\uparrow).

Method	BD-Quality \uparrow			
	LPIPS	DISTS	PSNR	MS-SSIM
MDIC w/o ($z_d + \hat{z}_{xc}$)	-0.3550	-0.1826	-8.6358	-6.5115
MDIC w/o z_d	-0.1179	-0.0489	-2.8161	-3.1127
MDIC (Ours)	0	0	0	0

The G_1 and G_2 in MG-SISM. As shown in Table 2, we perform ablation experiments on the G_1 and G_2 components within the MG-SISM to validate the effectiveness of our mask-gating mechanism. The results demonstrate that applying mask gating enables the model to better exploit visual side information during reconstruction, while effectively suppressing redundant and inconsistent multi-view

Table 2. The ablation of the mask-gate G_1 and G_2 . Symbol convention: \uparrow =higher better.

Method	BD-Quality \uparrow			
	LPIPS	DISTS	PSNR	MS-SSIM
MDIC w/o ($G_1 + G_2$)	-0.0437	-0.0050	-0.5979	-0.4491
MDIC w/o G_2	-0.0106	-0.0045	-0.2864	-0.2595
MDIC (Ours)	0	0	0	0

features. To further provide an intuitive understanding of the impact of our gating mechanism, Fig. 9 presents visual comparisons between two ablated variants and the MDIC. It is clear that incorporating the gating mechanism facilitates more accurate reconstruction of object boundaries and enhances consistency between category-level and fine-grained semantic details.

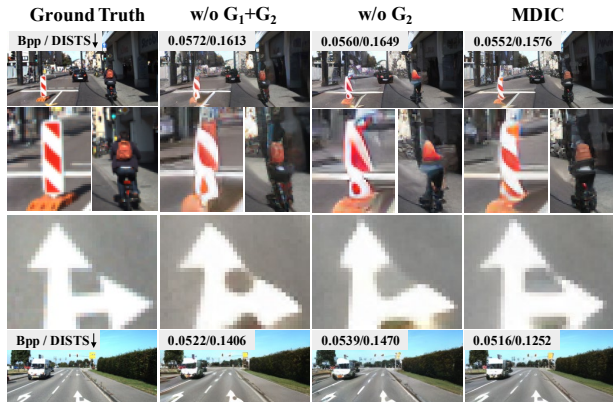


Figure 9. The visual comparison results after ablating the G_1 and G_2 in MG-SISM.

Additional experimental results on complexity, hyperparameters, and the role of multimodal side information are provided in the Supplementary Material.

5. Conclusion

In this paper, we propose an innovative Multimodal Distributed Image Compression (MDIC) framework that leverages multimodal side information and decodes compressed latent representations with a pre-trained text-to-image diffusion model. A text-supervised visual mask restores category semantics lost in VQ-VAE compression and extracts fine-grained details from visual side information, ensuring semantically faithful reconstruction. Extensive experiments demonstrate clear perceptual advantages over existing multi-view coding and diffusion-based methods. In the future, we will investigate stronger multi-view correlations and unified pre-trained decoders.

Acknowledgement

This work is partially supported by the Hubei Province Major Science and Technology Innovation Program (2024BAA011), the Key Research and Development Program of Hubei Province (2025BEB012, 2023BAB016).

References

- [1] Sharon Ayzik and Shai Avidan. Deep image compression using decoder side information. In *European Conference on Computer Vision*, pages 699–714. Springer, 2020. 2
- [2] Mikołaj Bińkowski, Danica J Sutherland, Michael Arbel, and Arthur Gretton. Demystifying mmd gans. *arXiv preprint arXiv:1801.01401*, 2018. 6
- [3] Marlene Careil, Matthew J Muckley, Jakob Verbeek, and Stéphane Lathuilière. Towards image compression with perfect realism at ultra-low bitrates. In *The Twelfth International Conference on Learning Representations*, 2023. 2, 3, 6, 7, 8
- [4] Marius Cordts, Mohamed Omran, Sebastian Ramos, Timo Rehfeld, Markus Enzweiler, Rodrigo Benenson, Uwe Franke, Stefan Roth, and Bernt Schiele. The cityscapes dataset for semantic urban scene understanding. In *Proceedings of the IEEE Conference on Computer Vision and Pattern Recognition*, pages 3213–3223, 2016. 6
- [5] Keyan Ding, Kede Ma, Shiqi Wang, and Eero P Simoncelli. Image quality assessment: Unifying structure and texture similarity. *IEEE Transactions on Pattern Analysis and Machine Intelligence*, 44(5):2567–2581, 2020. 6
- [6] Alexey Dosovitskiy, Lucas Beyer, Alexander Kolesnikov, Dirk Weissenborn, Xiaohua Zhai, Thomas Unterthiner, Mostafa Dehghani, Matthias Minderer, Georg Heigold, Sylvain Gelly, Jakob Uszkoreit, and Neil Houlsby. An image is worth 16x16 words: Transformers for image recognition at scale. In *9th International Conference on Learning Representations*, 2021. 5
- [7] Andreas Geiger, Philip Lenz, and Raquel Urtasun. Are we ready for autonomous driving? the kitti vision benchmark suite. In *2012 IEEE Conference on Computer Vision and Pattern Recognition*, pages 3354–3361, 2012. 6
- [8] Martin Heusel, Hubert Ramsauer, Thomas Unterthiner, Bernhard Nessler, and Sepp Hochreiter. Gans trained by a two time-scale update rule converge to a local nash equilibrium. *Advances in Neural Information Processing Systems*, 30, 2017. 6
- [9] Eric Jang, Shixiang Gu, and Ben Poole. Categorical reparameterization with gumbel-softmax. *arXiv preprint arXiv:1611.01144*, 2016. 5
- [10] Xuhao Jiang, Weimin Tan, Tian Tan, Bo Yan, and Liquan Shen. Multi-modality deep network for extreme learned image compression. In *Proceedings of the AAAI Conference on Artificial Intelligence*, pages 1033–1041, 2023. 2
- [11] Anle Ke, Xu Zhang, Tong Chen, Ming Lu, Chao Zhou, Jiawen Gu, and Zhan Ma. Ultra lowrate image compression with semantic residual coding and compression-aware diffusion. In *International Conference on Machine Learning*. PMLR, 2025. 2
- [12] Jari Korhonen and Junyong You. Peak signal-to-noise ratio revisited: Is simple beautiful? In *2012 Fourth International Workshop on Quality of Multimedia Experience*, pages 37–38, 2012. 3, 7
- [13] Junnan Li, Dongxu Li, Silvio Savarese, and Steven Hoi. Blip-2: Bootstrapping language-image pre-training with frozen image encoders and large language models. In *International Conference on Machine Learning*, pages 19730–19742. PMLR, 2023. 3, 4
- [14] Zhiyuan Li, Yanhui Zhou, Hao Wei, Chenyang Ge, and Jingwen Jiang. Towards extreme image compression with latent feature guidance and diffusion prior. *IEEE Transactions on Circuits and Systems for Video Technology*, 2024. 2, 3, 7
- [15] Zhiyuan Li, Yanhui Zhou, Hao Wei, Chenyang Ge, and Ajmal Mian. Rdeic: Accelerating diffusion-based extreme image compression with relay residual diffusion. *IEEE Transactions on Circuits and Systems for Video Technology*, pages 1–1, 2025. 2, 3, 7
- [16] Tsung-Yi Lin, Michael Maire, Serge Belongie, James Hays, Pietro Perona, Deva Ramanan, Piotr Dollár, and C Lawrence Zitnick. Microsoft coco: Common objects in context. In *European Conference on Computer Vision*, pages 740–755. Springer, 2014. 2
- [17] Zhening Liu, Xinjie Zhang, Jiawei Shao, Zehong Lin, and Jun Zhang. Bidirectional stereo image compression with cross-dimensional entropy model. In *European Conference on Computer Vision*, pages 480–496. Springer, 2024. 2, 3, 7
- [18] Jonathan Long, Evan Shelhamer, and Trevor Darrell. Fully convolutional networks for semantic segmentation. In *Proceedings of the IEEE Conference on Computer Vision and Pattern Recognition*, pages 3431–3440, 2015. 7
- [19] Yiyang Ma, Wenhan Yang, and Jiaying Liu. Correcting diffusion-based perceptual image compression with privileged end-to-end decoder. 2024. 2
- [20] Nitish Mital, Ezgi Özyilkan, Ali Garjani, and Deniz Gündüz. Neural distributed image compression using common information. In *2022 Data Compression Conference (DCC)*, pages 182–191. IEEE, 2022. 1, 2, 3, 6, 7
- [21] Nitish Mital, Ezgi Özyilkan, Ali Garjani, and Deniz Gündüz. Neural distributed image compression with cross-attention feature alignment. In *Proceedings of the IEEE/CVF Winter Conference on Applications of Computer Vision*, pages 2498–2507, 2023. 1, 2, 3, 7
- [22] Anish Mittal, Rajiv Soundararajan, and Alan C Bovik. Making a “completely blind” image quality analyzer. *IEEE Signal Processing Letters*, 20(3):209–212, 2012. 6
- [23] Guy Ohayon, Hila Manor, Tomer Michaeli, and Michael Elad. Compressed image generation with denoising diffusion codebook models. In *Forty-second International Conference on Machine Learning*, 2025. 2
- [24] Ya Qiao, Yongqi Zhai, and Ronggang Wang. Bssic: Stereo image compression based on block shift. In *2024 International Joint Conference on Neural Networks (IJCNN)*, pages 1–7. IEEE, 2024. 3
- [25] Shi-Yu Qin, Bin Chen, Yu-Jun Huang, Bao-Yi An, Tao Dai, and Shu-Tao Xia. Perceptual image compression with textual side information. *Pattern Recognition*, 169:111848, 2026. 2

- [26] Alec Radford, Jong Wook Kim, Chris Hallacy, Aditya Ramesh, Gabriel Goh, Sandhini Agarwal, Girish Sastry, Amanda Askell, Pamela Mishkin, Jack Clark, et al. Learning transferable visual models from natural language supervision. In *International Conference on Machine Learning*, pages 8748–8763. PMLR, 2021. 4
- [27] Robin Rombach, Andreas Blattmann, Dominik Lorenz, Patrick Esser, and Björn Ommer. High-resolution image synthesis with latent diffusion models. In *Proceedings of the IEEE/CVF Conference on Computer Vision and Pattern Recognition*, pages 10684–10695, 2022. 4
- [28] Olaf Ronneberger, Philipp Fischer, and Thomas Brox. U-net: Convolutional networks for biomedical image segmentation. In *International Conference on Medical Image Computing and Computer-Assisted Intervention*, pages 234–241. Springer, 2015. 6
- [29] David Slepian and Jack Wolf. Noiseless coding of correlated information sources. *IEEE Transactions on Information Theory*, 19(4):471–480, 1973. 1, 3
- [30] Aaron Van Den Oord, Oriol Vinyals, et al. Neural discrete representation learning. *Advances in Neural Information Processing Systems*, 30, 2017. 2, 3, 4
- [31] Zhou Wang, Eero P Simoncelli, and Alan C Bovik. Multiscale structural similarity for image quality assessment. In *The Thirty-seventh Asilomar Conference on Signals, Systems & Computers, 2003*, pages 1398–1402. IEEE, 2003. 3, 7
- [32] Jay Whang, Alliot Nagle, Anish Acharya, Hyeji Kim, and Alexandros G. Dimakis. Neural distributed source coding. *IEEE Journal on Selected Areas in Information Theory*, 5: 493–508, 2024. 1, 3, 4
- [33] Matthias Wödlinger, Jan Kotera, Jan Xu, and Robert Sablatnig. Sasic: Stereo image compression with latent shifts and stereo attention. In *Proceedings of the IEEE/CVF Conference on Computer Vision and Pattern Recognition*, pages 661–670, 2022. 3, 7
- [34] Matthias Wödlinger, Jan Kotera, Manuel Keglevic, Jan Xu, and Robert Sablatnig. Ecsic: Epipolar cross attention for stereo image compression. In *Proceedings of the IEEE/CVF Winter Conference on Applications of Computer Vision*, pages 3436–3445, 2024. 3, 7
- [35] Aaron Wyner and Jacob Ziv. The rate-distortion function for source coding with side information at the decoder. *IEEE Transactions on Information Theory*, 22(1):1–10, 2003. 1, 3
- [36] Ruihan Yang and Stephan Mandt. Lossy image compression with conditional diffusion models. *Advances in Neural Information Processing Systems*, 36:64971–64995, 2023. 2
- [37] Selim F Yilmaz, Ezgi Ozyilkan, Deniz Gündüz, and Elza Erkip. Distributed deep joint source-channel coding with decoder-only side information. In *2024 IEEE International Conference on Machine Learning for Communication and Networking (ICMLCN)*, pages 139–144. IEEE, 2024. 1
- [38] Yankai Yin, Zhe Sun, Peiying Ruan, Ruidong Li, and Feng Duan. Learned distributed image compression with decoder side information. *Digital Communications and Networks*, 11(2):349–358, 2025. 1, 2
- [39] Richard Zhang, Phillip Isola, Alexei A Efros, Eli Shechtman, and Oliver Wang. The unreasonable effectiveness of deep features as a perceptual metric. In *Proceedings of the IEEE Conference on Computer Vision and Pattern Recognition*, pages 586–595, 2018. 6
- [40] Xinjie Zhang, Jiawei Shao, and Jun Zhang. Ldmic: Learning-based distributed multi-view image coding. In *International Conference on Learning Representations*, 2023. 1, 2, 3, 7
- [41] Xinjie Zhang, Shenyuan Gao, Zhening Liu, Jiawei Shao, Xingtong Ge, Dailan He, Tongda Xu, Yan Wang, and Jun Zhang. Camsic: Content-aware masked image modeling transformer for stereo image compression. In *Proceedings of the AAAI Conference on Artificial Intelligence*, pages 10239–10247, 2025. 2, 3, 7
- [42] Lingyu Zhu, Xiangrui Zeng, Bolin Chen, Peilin Chen, Yung-Hui Li, and Shiqi Wang. Leveraging diffusion knowledge for generative image compression with fractal frequency-aware band learning. *arXiv preprint arXiv:2503.11321*, 2025. 2